Modal S-matrix method for the optimum design of inductively direct-coupled cavity filters

Prof. F. Arndt, Dr.-Ing., Sen.Mem.I.E.E.E., J. Bornemann, Dr.-Ing., D. Heckmann, Dipl.-Ing., C. Piontek, Dipl.-Ing., H. Semmerow, Dipl.-Ing., and H. Schueler, Dipl.-Ing.

Indexing terms: *Computer-aided design, Waveguides*

Abstract: A rigorous field theory method is described for the computer-aided design of a class of rectangular waveguide filters, where the cavities are coupled by irises, *E*-plane integrated metal inserts, broadside oriented strip obstacles, or multiple quadratic posts. These coupling elements enable low-cost manufacturing, since accurate and inexpensive metal-etching techniques, or materials with standard dimensions may be utilised. The design method is based on field expansion in suitably normalised eigenmodes which yield directly the modal scattering matrix of two appropriate key building blocks for this kind of filter, the step-wall discontinuity and the *N*-furcated waveguide section of finite length. The theory includes the finite thickness of the diaphragms, strips or posts as well as the immediate higher-order mode interaction of all discontinuities. The stop-band characteristic of the filter is taken into account in the optimisation process. Optimised data are given for Ku-, E-, W-, and D-band filter examples, whereby it is shown that the theory is also very appropriate for broadband designs. The theory is verified by measured results for a six resonator iris coupled Ku-band filter, with a midband frequency of 15.2 GHz and a seven-resonator metal insert D-band filter, with a midband frequency of 142.5 GHz, showing measured minimum insertion losses of 0.2 dB and 1.4 dB, respectively.

1 Introduction

Shunt-inductive coupling of cavities by irises or obstacles is a common technique extensively employed in the industry to produce waveguide bandpass filters for a wide variety of applications [1–31]. Although many refined design procedures are available, based on conventional impedance inverter and lowpass prototype techniques [2–13], as well as on improved equivalent circuit models [2–16], increasing activity at millimetre-wave frequencies [17–28] has encouraged interest in exact field theory methods which allow accurate computer-aided filter design, taking into account both the finite thickness of the obstacles and the higher-order mode interaction between them. Moreover, with the growing demand for such components to be applied for integrated circuits purposes, such as for convertors, diplexers, or complete front-ends [17–24], for good overall performance, the inclusion of stop-band characteristics in the design process becomes increasingly important.

The purpose of this paper is to achieve a suitable field-theory computer-aided design method for the class of waveguide filters shown in Fig. 1, where the cavities are coupled inductively by irises, *E*-plane integrated metal inserts, broadside strips or multiple quadratic posts. As accurate and inexpensive metal-etching techniques, or materials with standard dimensions may be utilised, the exact design theory enables the high-precision low-cost manufacturing of low-insertion-loss bandpass filters without the necessity for additional 'trial-and-error' adjustment methods. High attenuation requirements over a broad second stopband may be met by a suitable choice of the coupling elements, or cavity dimensions: multiple inserts [26, 29] may help to alleviate the direct coupling of modes along the strip sections; cavities with decreased cut-off frequency [30] diminish the influence of the nonlinear relation between frequency and guide wavelengths. Moreover, the inductive step-wall discontinuity junction effect is utilised as an additional design parameter.

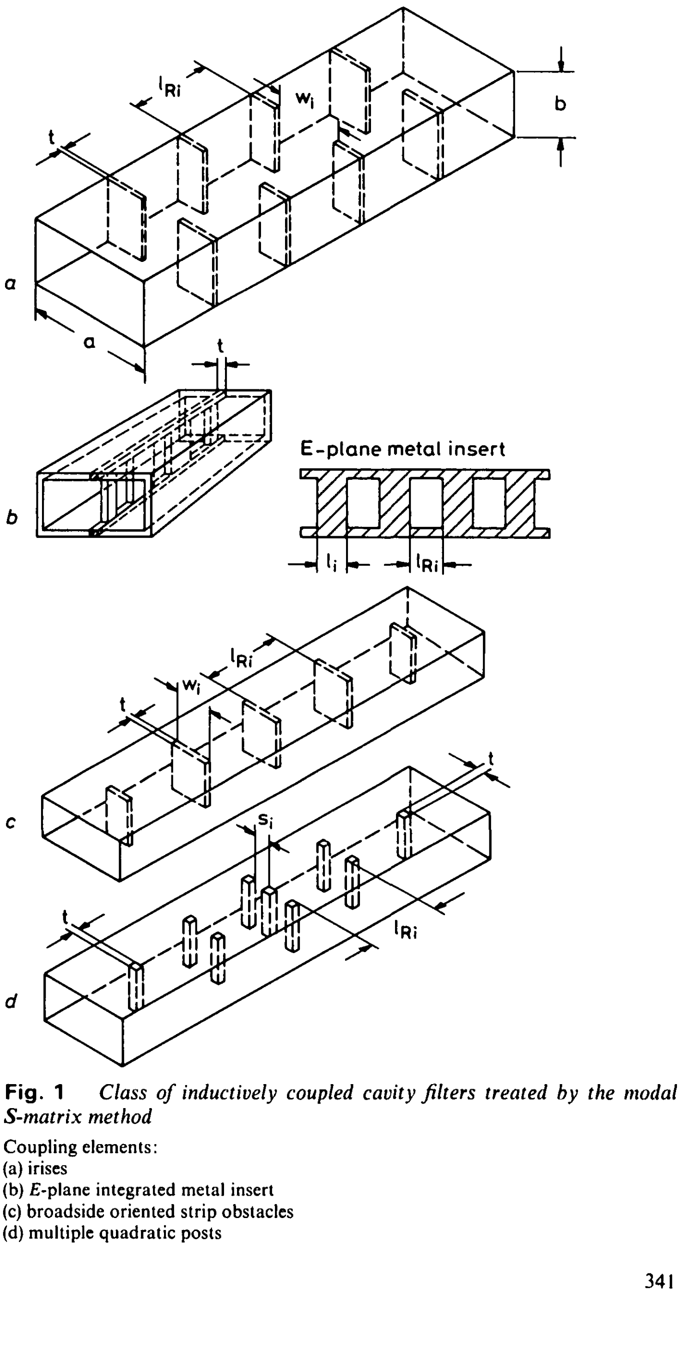

Fig. 1 *Class of inductively coupled cavity filters treated by the modal S-matrix method*

Coupling elements:
(a) irises
(b) *E*-plane integrated metal insert
(c) broadside oriented strip obstacles
(d) multiple quadratic posts

Paper 4839H (E12, C6), first received 3rd April and in revised form 4th July 1986

The authors are with the Microwave Department, University of Bremen, Kufsteiner Strasse, NW-1, D-2800 Bremen 33, West Germany

Many excellent papers on the field theory treatment of waveguide discontinuities are available, e.g. References 32–44, including wideband network modelling of interacting inductive irises [42–44]. The computer-aided design method in this paper, however, is based on field expansion into normalised eigenmodes [45] which yield directly the modal S-matrix [25–31] of two key building-block discontinuities. The immediate modal S-matrix combination of all interacting structures includes the higher-order mode coupling effects, the finite thicknesses of all obstacles, and allows the stopband characteristic to be included in the filter design. For computer optimisation, the evolution strategy method [28, 46], i.e. a suitably modified direct-search procedure, is applied where no differentiation step in the optimisation process is necessary and hence the problem of local minima may be circumvented. Coupling integrals in the orthogonality relations of the field expansion can be evaluated analytically, and only a modest number of waveguide modes is required to achieve satisfactory convergence. This reduces the computing time involved considerably.

The method of field expansion into suitably normalised eigenmodes has already been applied successfully by some of the authors for analysing and designing various waveguiding structures, see References 25–31 and 45. This paper compiles those aspects of the theory which are relevant for designing the class of inductively direct-coupled cavity filters shown in Fig. 1. The modal S-matrix elements for the change in waveguide width (key building block of iris coupled filters and of filters within increased or decreased cavities) and for the H-plane N-furcated waveguide of finite length (key building block of inductive obstacle coupled filter) are explicitly reproduced, therefore. To demonstrate the effect of higher-order mode coupling along the filter section, the results of the rigorous field-theory method are compared with those of the usual equivalent network theory [3], which ignores that influence, at the example of a common Ku-band (12–18 GHz) iris coupled filter. W-band (75–110 GHz) E-plane metal insert filters with ultrabroad second stopband are designed, showing that principles of Ku-band (12–18 GHz) and Ka-band (26–40 GHz) filter designs [26, 29, 30] may also be applied to millimetre waves. Compact filters with improved second stopband are obtained utilising broadside oriented metal-strip obstacles and triple-strip sections combined with broadside oriented strips. The numerical design of optimum filters includes a type of multiple post coupling elements, which has the advantage of being producible by materials with standard dimensions (quadratic posts, or round posts, as circular to quadratic cross-section equivalence relations [1] may be utilised). Moreover, it is demonstrated that the exact modal S-matrix method described may be applied directly for the optimum design of metal insert filters with broad passbands exceeding the otherwise critical value of five percent [50], and also for filters with passbands at very high frequencies.

Design examples for optimised Ku- (12–18 GHz), Ka- (26–40 GHz), E- (60–90 GHz), W- (75–110 GHz) and D-band (110–170 GHz) filters are given. The theory is experimentally verified by measured results for a six-resonator iris coupled Ku-band filter, and a new broadband low-insertion-loss E-plane integrated all-metal insert D-band filter.

2 Theory

For the computer-aided design of the inductively direct-coupled cavity filters (Fig. 1), the modal S-matrix method [25–31] is applied. The technique proves to be ideally suited to computers, involving mainly the solution of sets of simultaneous linear equations. For calculation of the scattering matrix, the filter is decomposed into two key building blocks (Fig. 2): the abrupt change in waveguide width (Fig. 2a), for the iris coupled filter type (Fig. 1a); the H-plane N-furcation (Fig. 2c), for the E-plane metal-insert (with $N = 2$) and $N - 1$ inductive obstacle coupled filters

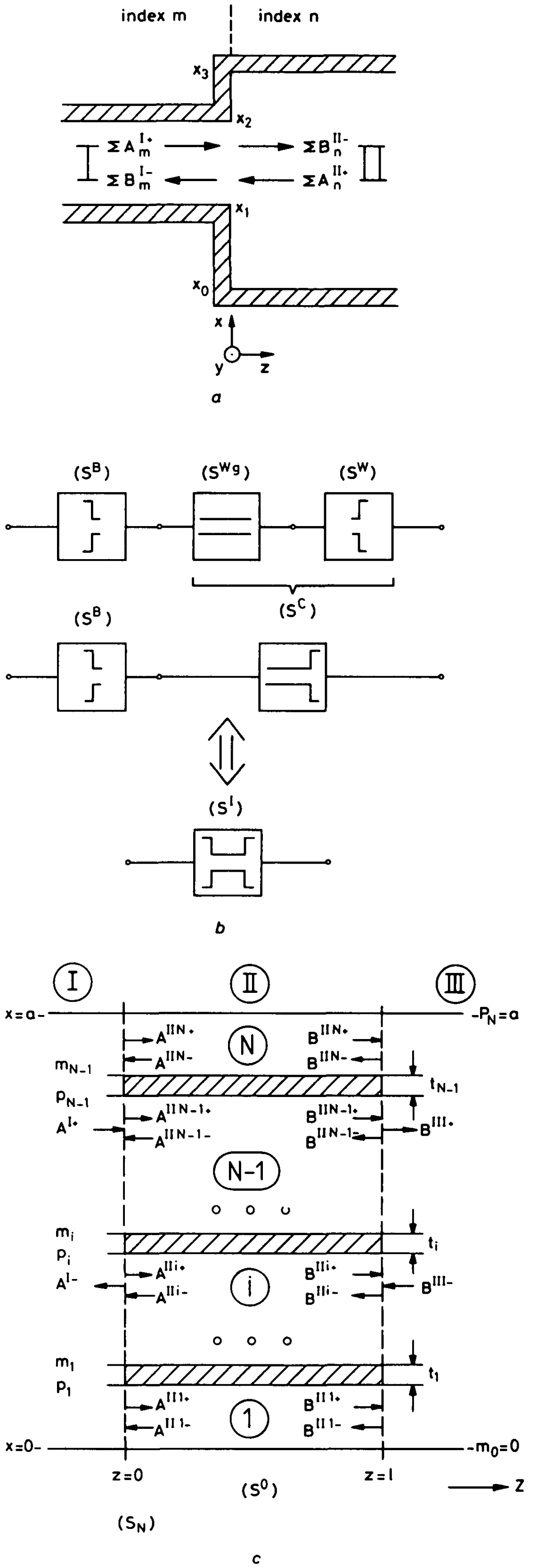

Fig. 2 *Key building blocks for the rigorous field theory analysis*
a Step-wall discontinuity
b Composed scattering matrices for the iris of finite thickness
c N-furcated waveguide of finite length

(Figs. 1b–1d). Combination with the known scattering matrices of the corresponding intermediate homogeneous waveguide sections (e.g. (S^{Wg}) in Fig. 2b) yields the total scattering matrix for the corresponding coupling element (e.g. the iris (S^I) in Fig. 2b), or the $N-1$ inductive obstacles (e.g. (S^0) of the N-furcated waveguide section in Fig. 2c). Note that for the inverse structure, the related scattering matrix (e.g. (S^B) in Fig. 2b) is simply derived by merely interchanging the corresponding submatrix elements of the initially computed matrix (e.g. of (S^W)) of the original structure (cf. Fig. 2a). The overall scattering matrix of the total filter is then calculated by a suitable direct combination of all single modal scattering matrices of eqn. 19, Appendix 7.3.

Inductive obstacles coupled filters with additional abrupt change in waveguide width (for improved stopband behaviour, cf. Fig. 6) require the inclusion of both key building blocks (Figs. 2a and 2c).

For the homogeneous waveguide subregions $v = \mathrm{I}, \mathrm{II}$ (Fig. 2a), or $v = \mathrm{I}, \mathrm{II1}, \mathrm{II2}, \mathrm{II3}, \ldots, \mathrm{IIi}, \ldots, \mathrm{IIN}$ (Fig. 2c) the fields [32] at $z = 0$

$$\boldsymbol{E}^{(v)} = -j\omega\mu\nabla \times \boldsymbol{\Pi}_{hx}^{(v)}, \quad \boldsymbol{H}^{(v)} = \nabla \times \nabla \times \boldsymbol{\Pi}_{hx}^{(v)} \tag{1}$$

are derived from the x-component of the magnetic Hertzian vector potential $\boldsymbol{\Pi}_h$, which is assumed to be the sum of the rectangular waveguide eigenmodes [25–33] satisfying the Helmholtz equation, and the boundary conditions at the metallic surfaces (Fig. 2c)

$$\boldsymbol{\Pi}_{hx}^{(v)} = \boldsymbol{e}_x \cdot \sum_{m=1}^{M} T_m^{(v)} \sin\left\{\frac{m\pi}{p^{(v)}} \cdot f^{(v)}\right\} \cdot [A_m^{(v)+} - A_m^{(v)-}] \tag{2}$$

The still unknown eigenmode amplitude coefficients $A^{(v)\pm}$ of the forward (+) and backward (−) waves are suitably normalised [32] by $T_m^{(v)}$, with regard to the complex power carried by each wave, to yield directly the corresponding modal scattering matrix at the discontinuity under consideration. The abbreviations in eqn. 2 are elucidated in the Appendix.

Matching the tangential field components E_y and H_x calculated by eqns. 1 and 2 for each of the two key building block discontinuities (Figs. 2a and 2c) at $z = 0$, and utilising the known orthogonality property of the related eigenfunctions [32, 33], yields the corresponding two modal scattering matrices for the two discontinuities. The modal scattering matrix $(\boldsymbol{S}^W)$ for the change in waveguide width (Fig. 2a) is then found to be

$$(\boldsymbol{S}^W) = \begin{pmatrix} (S_{11}^W) & (S_{12}^W) \\ (S_{21}^W) & (S_{22}^W) \end{pmatrix}, \tag{3}$$

where the submatrices are given explicitly in the Appendix.

The scattering matrix of two series connected structures (e.g. $(\boldsymbol{S}^{Wg})$ and $(\boldsymbol{S}^W)$ in Fig. 2b) is calculated by combining directly the single scattering matrices. Contrary to the usual treatment with transmission matrices, this procedure preserves numerical accuracy, since the expressions contain exponential functions with only negative argument. This avoids numerical instabilities caused by the otherwise known situation of interacting discontinuities if evanescent modes are involved. A further advantage is that no symmetry of ports (i.e. modes) is required. Therefore, there is no need to maintain the number of 'localised' [47] modes, necessary for calculating the scattering matrix of the step discontinuity, for the 'accessible' [48] modes with a homogeneous waveguide section between them. The utilisation of this non-symmetry helps to reduce computing time and storage requirements. For completeness, the scattering coefficients for two series connected sections are given in the Appendix. The scattering matrix for more sections is found analogously using this equation iteratively.

The modal scattering matrix $(\boldsymbol{S}^I)$ of the iris of finite thickness t (Fig. 2b) is calculated using the scattering matrix, eqn. 3, the scattering matrix of the inverse structure $(\boldsymbol{S}^B)$

$$(\boldsymbol{S}^B) = \begin{pmatrix} (S_{11}^B) & (S_{12}^B) \\ (S_{21}^B) & (S_{22}^B) \end{pmatrix} = \begin{pmatrix} (S_{22}^W) & (S_{21}^W) \\ (S_{12}^W) & (S_{11}^W) \end{pmatrix} \tag{4}$$

and the scattering matrix of the homogeneous waveguide section of finite length t

$$(\boldsymbol{S}^{Wg}) = \begin{pmatrix} (0) & (\boldsymbol{E}) \\ (\boldsymbol{E}) & (0) \end{pmatrix} \tag{5}$$

with the diagonal matrices $(\boldsymbol{E})$ containing the propagation factors k_{zm} (see eqn. 17)

$$(\boldsymbol{E}) = \begin{pmatrix} e^{-jk_{z1}t} & 0 \\ 0 & e^{-jk_{zm}t} \end{pmatrix} \tag{6}$$

in the manner shown in Fig. 2b, utilising eqn. 19:

$$(\boldsymbol{S}^I) = \begin{pmatrix} (S_{11}^I) & (S_{12}^I) \\ (S_{21}^I) & (S_{22}^I) \end{pmatrix} \tag{7}$$

where the submatrices are elucidated in the Appendix.

Utilising the similar procedure of field matching at $z = 0$ and direct combination of the involved scattering matrices, the modal scattering matrix $(\boldsymbol{S}^0)$ of the $N-1$ inductive obstacle section of finite length l (Fig. 2c) is given by

$$(\boldsymbol{S}^0) = \begin{pmatrix} (S_{11}^0) & (S_{12}^0) \\ (S_{21}^0) & (S_{22}^0) \end{pmatrix} \tag{9}$$

with the submatrices given in the Appendix.

For the calculations of the paper, the expansion into fifteen eigenmodes at each discontinuity yields sufficient convergence behaviour of the scattering coefficient. If 'accessible' modes of reduced number are utilised for usual cavity lengths, only the propagating modes and the first few evanescent modes are necessary. The final design data are checked by up to 45 eigenmodes.

The design theory described allows the assessment of the midband dissipation loss of the filters. The attenuation along the waveguide sections may be included in the corresponding diagonal matrices (cf. eqn. 6) by introducing complex propagation factors. The attenuation factor can be calculated by the estimated or measured resonator Qs for the type of filter construction proposed, following the considerations for lowpass prototype filters given in Reference 3. Measured Qs of grounded finline resonators, for example, which correspond for lower frequency ranges approximately to those of all-metal constructions, may be found in Reference 18.

Moreover, tolerance sensitivity simulations may be easily done by introducing measured or estimated deviations from optimised design data in the exact analysis procedure. As no iteration process is required for this, the overall insertion loss for given parameters may be calculated with a high number of eigenmodes. Excellent agreement between theoretically predicted and measured filter response may be observed, therefore, if the deviations from the optimised design data are measured accurately, e.g. by means of a measuring microscope.

3 Optimisation procedure

The computer-aided design is carried out by an optimisation program which applies the evolution strategy method [28, 46]. An error function $F(\bar{x})$ to be minimised is defined (Fig. 3)

$$F(\bar{x}) = \sum_{v=1}^{V_{stop}} \{a_{smin}/a_{21}(f_v)\}^2 + \sum_{v=1}^{V_{pass}} \{a_{21}(f_v)/a_{pmax}\}^2 \tag{10}$$

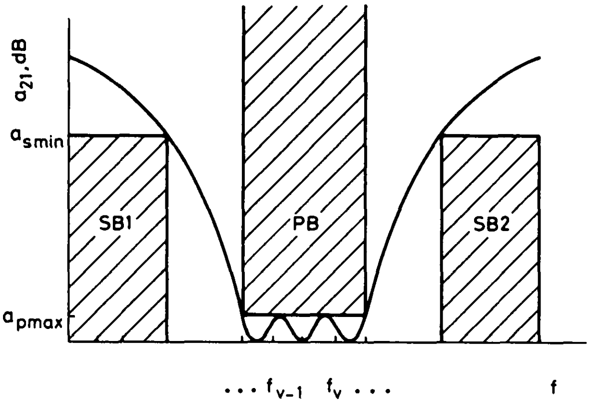

Fig. 3 *Scheme for the computer optimisation*

where f_v are the frequency sample points, and V_{stop} and V_{pass} are the number of sample points in stopbands SB1, SB2, and passband PB, respectively. A number of 20–30 frequency sample points, both in passband and stopband, has turned out to be sufficient. Values a_{smin} and a_{pmax} are the given minimum stopband and maximum passband attenuation, respectively, and $a_{21} = -20 \log (|S_{21}|)$ is the insertion loss at the frequency f_v, calculated according to Section 2.

For given waveguide housing dimensions a, b and thickness t of the irises or inductive obstacles and number of resonators, respectively, the parameters $\bar{x}$ to be optimised are all resonator lengths l_{Ri} and widths w_i of the iris apertures (see Fig. 1*a*), or inductive obstacles (see Fig. 1*c*), or lengths l_i of the *E*-plane inserts (see Fig. 1*b*), or spacings s_i of the multiple posts (see Fig. 1*d*). The initial values for the resonator lengths for the optimisation procedure may be chosen to be $\lambda_g/3$ to $\lambda_g/2$, where λ_g is the guide wavelength of the H_{10}-mode at the given midband frequency. A more favourable approximation, however, concerning computing time, is the network theory synthesis approach according to Reference 3. In order to reduce the number of parameters, the filters are assumed to be symmetrical with regard to half of the total filter structure.

A main optimisation strategy parameter H, a secondary strategy parameter G and a standard random variable $r \in (-1, +1)$ influence [46] the alternation of the parameter $(\bar{x})$ during the optimisation process with the standard deviation $\sigma = H \cdot G$. The new parameters $(\bar{x})_{new}$ are calculated at each iteration step by

$$(\bar{x})_{new} = (\bar{x})_{old} - r \cdot (\bar{x})_{old} \cdot \sigma \tag{11}$$

where $(\bar{x})_{old}$ are the preceding parameters. Initial values for H and G are chosen to be $H = 0.01$, $G = 1$. It is often convenient to adapt G to the individual parameters $\bar{x}$, i.e. the resonator length variation should be less than the variation of the coupling sections, if, for instance, the ripple behaviour has to be improved while the midband frequency behaviour of the filter is already satisfactory. After a successful trial, H is doubled; for more than three unsuccessful trials, H is halved. If the error function $F(\bar{x})$ is minimised three times by less than 0.2%, the result is interpreted as a local minimum. H is then multiplied by 10^4. So the optimisation process begins again for a different, perhaps better, parameter range, and the global minimum, if it differs from the local one already found, can be attained. To maintain physically realistic parameters, an appropriate variable transformation [46] is utilised.

4 Results

Fig. 4 shows the calculated insertion loss ($a = 20 \log (1/|S_{21}|)$) in decibels as a function of frequency for a four-

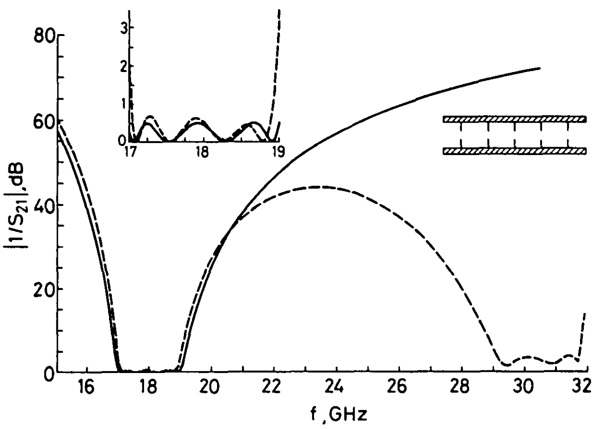

Fig. 4 *Iris-coupled filter*
- - - - rigorous theory
——— equivalent network theory
Filter dimensions (cf. Fig. 1*a*):
Waveguide housing $a = 15.799$ mm, $b = 7.899$ mm (Ku-band, R140)
Resonator lengths $l_{R1} = l_{R4} = 8.191$ mm, $l_{R2} = l_{R3} = 8.884$ mm
Iris widths $w_1 = w_5 = 6.080$ mm, $w_2 = w_4 = 4.278$ mm, $w_3 = 4.010$ mm
Iris thicknesses $t = 190$ μm

resonator iris filter. The solid line corresponds to results of an equivalent network synthesis procedure according to Reference 3. The dashed line represents the insertion loss calculated by the rigorous theory described in chapter 2. The influence of the higher-order mode coupling effect is obvious: the maximum stopband attenuation is only about 45 dB, and the second passband already exists at about 30 GHz.

As has been introduced recently [30], the stopband attenuation behaviour for iris-coupled cavity filters may be improved by increased resonator width $a' > a$ (Fig. 5). This is mainly due to the lowered fundamental mode cutoff frequency of the resonator section which modifies advantageously the nonlinear relation between guide wavelength λ_g and frequency; the next resonance at about $2(\lambda_g/2)$ of the halfwave resonators, therefore tends towards higher frequencies. This is demonstrated in Fig. 5*a* by a Ku-band four-resonator iris-coupled filter example. A second effect which is favourable for better stopband attenuation is that some iris apertures for increased-width sections are smaller than their normal section counterparts (identical passband behaviour provided). Moreover, the increased-width resonator filters lead to a reduction of the overall filter length. The commercially available iris sheet-metal thickness of $t = 190$ μm is very appropriate for exact production by photoetching techniques (cf. also the measured curve in Fig. 10).

The tolerance sensitivity of the filter is illustrated in Figs. 5*b*–5*e* at a three-resonator Ka-band design example. If the iris apertures deviate by $+0.02$ mm or -0.02 mm from the optimised values, only a relatively slight displacement of the filter response may be perceived (Fig. 5*b*). A frequency deviation of the passband is obtained by altering all resonator dimensions by the same deviation, e.g. the lengths by −0.04 mm (Figs. 5*c*) or the widths by −0.04 mm (Fig. 5*e*). A more severe influence is caused by a deviation from the optimum resonator lengths with different signs, e.g. resonator 1 and 3 by −0.04 mm, and resonator 2 by +0.04 mm (Fig. 5*d*): a frequency deviation of the passband, as well as a deterioration of the ripple behaviour, is obtained. In principle, these statements also hold for the other kind of filters investigated in this paper: the most critical parameters are the resonator lengths. Production techniques which may take advantage of metal-etching fabrication are particularly indicated for millimetre-wave designs, therefore. The optimum design procedure given in this paper may help to meet these requirements.

All-metal inserts mounted in the *E*-plane of rectangular waveguides (Figs. 1*a* and 6) yield low-cost mass-producible millimetre-wave filters with low passband insertion loss [18, 19, 25–30, 49]. The stopband attenuation behaviour of such filters may be improved by replacing the single strips by double- [26], or triple-strip sections [29]. This performance helps to circumvent the otherwise critical coupling of modes along the single-strip sections, with progressing frequency, if the distance between the strip and the waveguide sidewall is no longer negligible compared with the guide wavelength. Ultra-broadband stopband attenuation may be achieved by utilising, additionally, increased-width resonator sections in due combination with multiple-strip sections. This is shown in Fig. 6*a* by a W-band (75–110 GHz) metal-insert filter. The triple metal-insert filter with increased-width cavities yields a minimum stopband attenuation of about 65 dB between 91 and 117 GHz. For comparison, Fig. 6*a* also presents the calculated insertion losses of the corresponding double-insert (dashed-line) and single-insert filter (dash-dotted) line.

For metal-insert filters with passbands near the upper limit of the waveguide band, where the influence of direct coupling of modes along the strip sections dominates over the effect of the nonlinear relation between guide wavelength and frequency, improved stopband attenuation may be provided by merely reducing the distance between the strips and the waveguide sidewalls. This is demonstrated in Fig. 6*b* with the example of an E-band (60–90 GHz) filter.

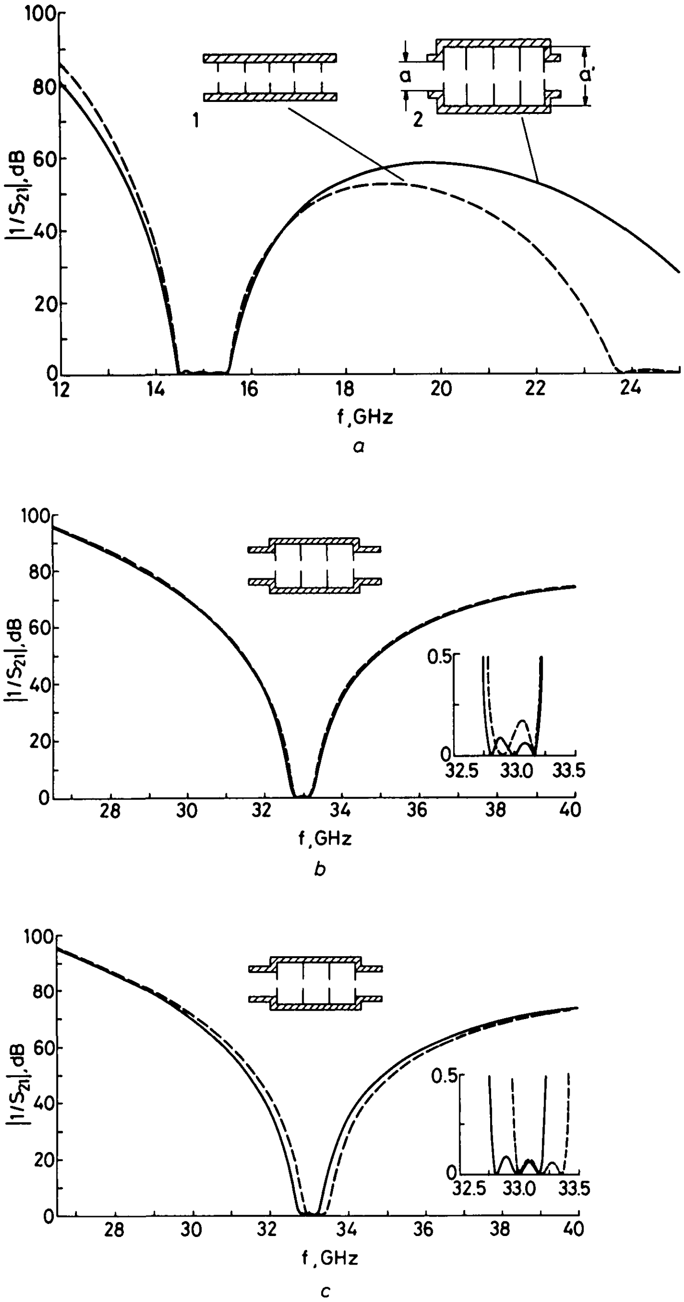

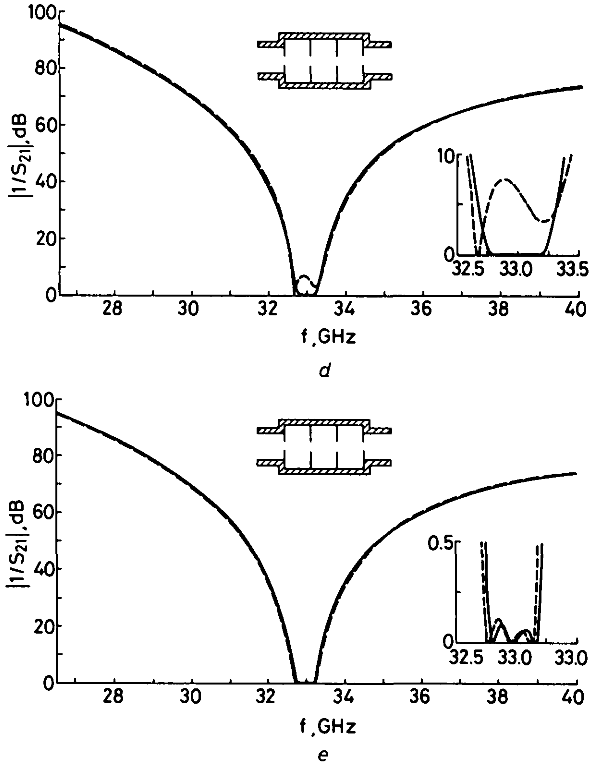

Fig. 5 *Iris-coupled filter with improved stopband attenuation*

a Filter dimensions (cf. Fig. 1*a*):
Waveguide housing a = 15.799 mm, b = 7.899 mm (Ku-band, R140)
Increased width a' = 20.538 mm; resonator lengths
- - - - filter 1
$l_{R1} = l_{R4}$ = 11.061 mm, $l_{R2} = l_{R3}$ = 11.911 mm
——— filter 2
$l_{R1} = l_{R4}$ = 9.981 mm, $l_{R2} = l_{R3}$ = 10.720 mm
Iris widths, filter 1, $w_1 = w_5$ = 6.406 mm, $w_2 = w_4$ = 4.286 mm, w_3 = 4.042 mm, filter 2, $w_1 = w_5$ = 6.484 mm, $w_2 = w_4$ = 4.140 mm, w_3 = 3.760 mm; iris thicknesses t = 190 μm
b Tolerance sensitivity simulation:
Deviations of the iris apertures by +0.02 mm (iris 1 and 4), and by −0.02 mm (iris 2 and 3).
Filter dimensions (optimised parameters): a = 7.112 mm, b = 3.556 mm (Ka-band, R320); a' = 9.246 mm; $l_{R1} = l_{R3}$ = 4.864 mm, l_{R2} = 5.101 mm; $w_1 = w_4$ = 2.416 mm, $w_2 = w_3$ = 1.176 mm
c Tolerance sensitivity simulation:
Deviations of all resonator lengths by −0.04 mm
d Tolerance sensitivity simulation:
Deviation of resonators no. 1 and 3 by −0.04 mm, and of resonator no. 2 by +0.04 mm
e Tolerance sensitivity simulation:
Deviation of all resonator widths by −0.04 mm

The tolerance sensitivity of the typical millimetre-wave all-metal finline filter (Fig. 6*a*, curve 1) is illustrated in Figs. 6*c*–6*d*. Fig. 6*c* shows an expanded view of the filter response, including the return loss, using the optimum design data given in Fig. 6*a*, curve 1. If each of the lengths of the metal inserts are decreased by 0.01 mm, a displacement of the passband by −170 MHz in frequency as well as a deterioration of the ripple behaviour (indicated by the return loss) may be perceived, since the metal insert lengths also account for the effective resonator lengths (Fig. 6*d*).

As has been described in Reference 29, broadside oriented metal strip obstacles provide better stopband attenuation than a single quadratic post of equivalent susceptance. This is also due to the reduced effect of direct coupling of modes, since the gap between the waveguide sidewalls and the strip obstacles is smaller than that one of a quadratic post. Fig. 7 shows an example of a six-resonator Ku-band broadside oriented strip obstacle filter providing a very broadband stopband attenuation.

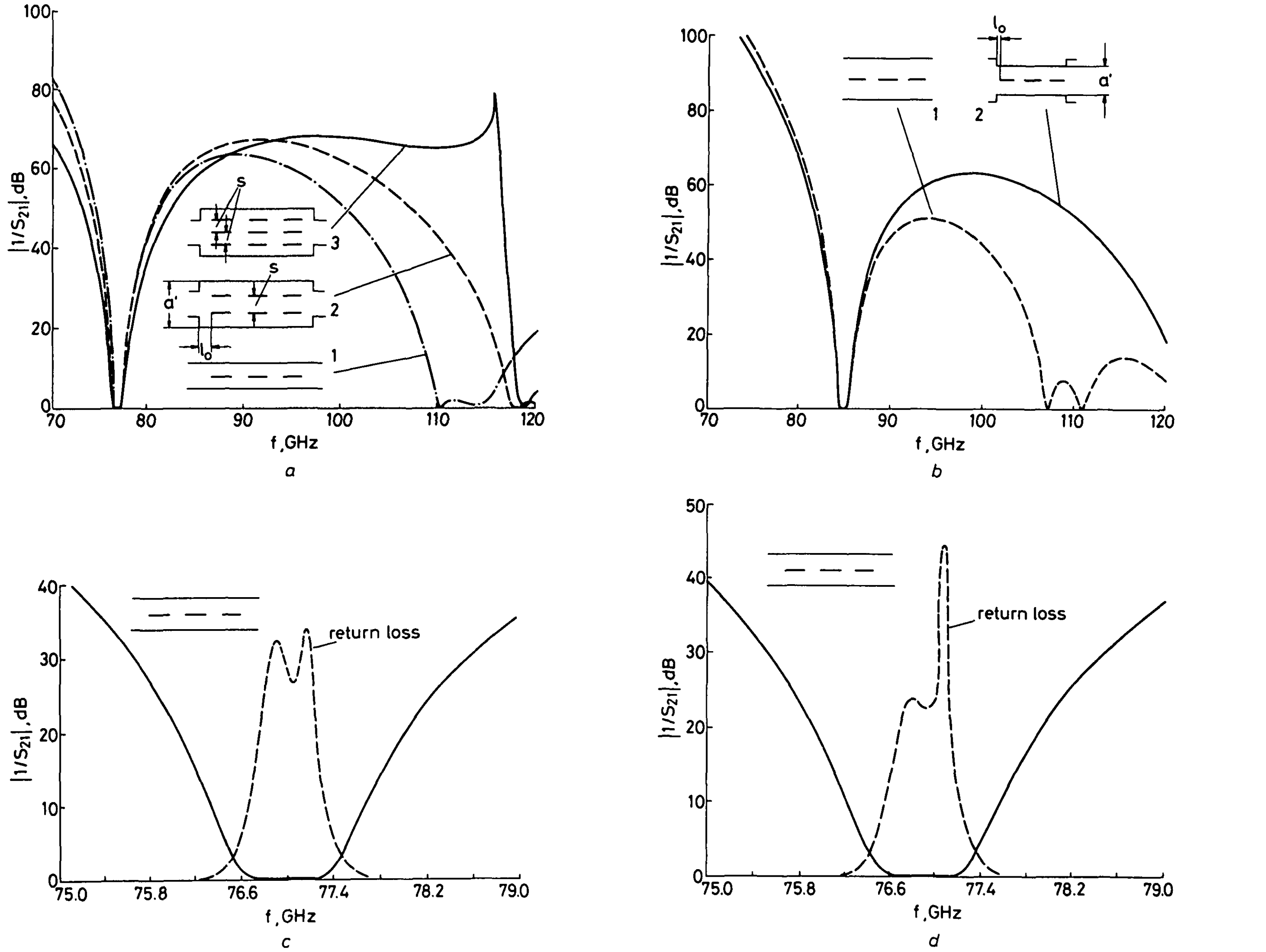

Fig. 6 *E-plane integrated metal-insert filters with improved stopband attenuation*

a W-band filter
Filter dimensions (cf. Fig. 1*b*)
Waveguide housing $a = 2.540$ mm, $b = 1.270$ mm (W-band, R900), insert thickness $t = 50\ \mu$m.
·—·—· Filter 1
Resonator lengths $l_{R1} = l_{R3} = 2.450$ mm, $l_{R2} = 2.477$ mm, insert lengths $l_1 = l_4 = 0.277$ mm, $l_2 = l_3 = 1.191$ mm.
– – – – Filter 2
$l_{R1} = l_{R3} = 2.336$ mm, $l_{R2} = 2.368$ mm, $l_1 = l_4 = 0.088$ mm, $l_2 = l_3 = 0.855$ mm, $l_0 = 2.289$ mm, $a' = 2.790$ mm, $s = 0.4$ mm.
——— Filter 3
$l_{R1} = l_{R3} = 1.827$ mm, $l_{R2} = 1.849$ mm, $l_1 = l_4 = 0.122$ mm, $l_2 = l_3 = 0.990$ mm, $l_0 = 1.971$ mm, $a' = 4.110$ mm, $s = 0.710$ mm
b E-band filter.
Filter dimensions (cf. Fig. 1*b*): Waveguide housing $a = 3.099$ mm, $b = 1.549$ mm (E-band, R740).
– – – – Filter 1
Insert thickness $t = 100\ \mu$m, resonator lengths $l_{R1} = l_{R3} = 1.406$ mm, $l_{R2} = 1.399$ mm, insert lengths $l_1 = l_4 = 0.858$ mm, $l_2 = l_3 = 2.712$ mm
——— Filter 2
Insert thickness $t = 50\ \mu$m, $l_{R1} = l_{R3} = 1.868$ mm, $l_{R2} = 1.877$ mm, $l_1 = l_4 = 0.437$ mm, $l_2 = l_3 = 1.514$ mm, $l_0 = 1.981$ mm, $a' = 2.540$ mm.
c W-band filter (cf. Fig. 6*a*), curve 1.
Expanded view
d Tolerance sensitivity simulation:
W-band filter (cf. Fig. 6*a*), curve 1.
All the metal inserts are decreased by −0.01 mm (i.e. all resonator lengths are increased by +0.01 mm, simultaneously)

Multiple-post coupled filters (Fig. 1*d*) have the advantage of being producible by materials with standard dimensions: e.g. quadratic posts or round posts, utilising the circular to rectangular cross-section equivalence relations [1] of inductive posts. Fig. 8 presents a Ku-band six-resonator filter example.

The good stopband attenuation properties of broadside oriented strip obstacles and triple-insert sections may be combined. This is demonstrated in Fig. 9 at a Ku-band filter example which yields a stopband attenuation of about 65 dB, although only two resonators are employed.

The calculated and measured insertion loss of a Ku-band iris-coupled six-resonator filter is shown in Fig. 10. The irises have been fabricated by metal-etching techniques. The material of the 190 μm-thick sheet-metals is 99.9% pure copper. The calculated midband dissipation

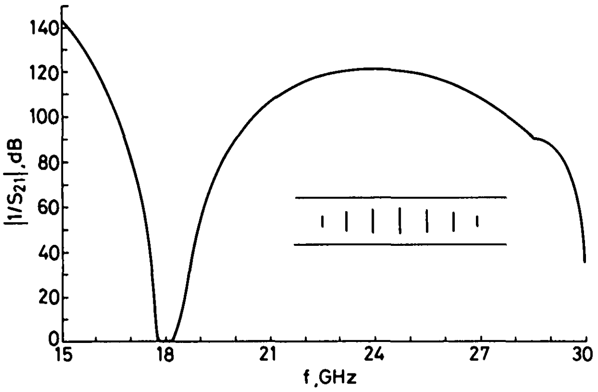

Fig. 7 *Broadside oriented metal strip obstacle coupled filter*

Filter dimensions (cf. Fig. 1*c*):
Waveguide housing a = 15.799 mm, b = 7.899 mm (Ku-band, R140)
Obstacle thickness t = 190 μm
Resonator lengths $l_1 = l_6$ = 8.662 mm, $l_2 = l_5$ = 9.493 mm, $l_3 = l_4$ = 9.588 mm
Obstacle widths $w_1 = w_7$ = 3.274 mm, $w_2 = w_6$ = 7.424 mm, $w_3 = w_5$ = 8.464 mm, w_4 = 8.466 mm

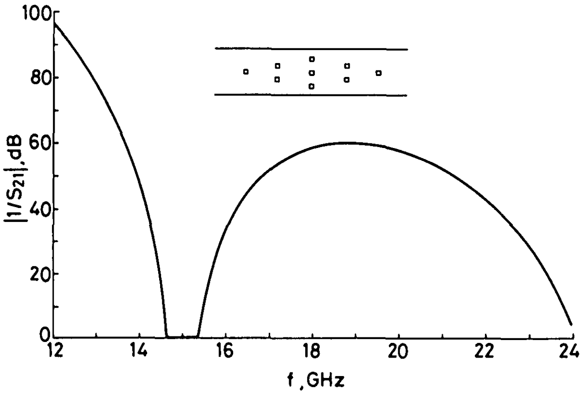

Fig. 8 *Multiple quadratic post coupled filter*

Filter dimensions (cf. Fig. 1*d*):
Waveguide housing a = 15.799 mm, b = 7.899 mm (Ku-band, R140)
Post dimensions 1 mm × 1 mm
Resonator lengths $l_{R1} = l_{R4}$ = 10.201 mm, $l_{R2} = l_{R3}$ = 11.631 mm
Post spacing s_1 = 3.576 mm (two posts), s_2 = 3.696 mm (three posts)

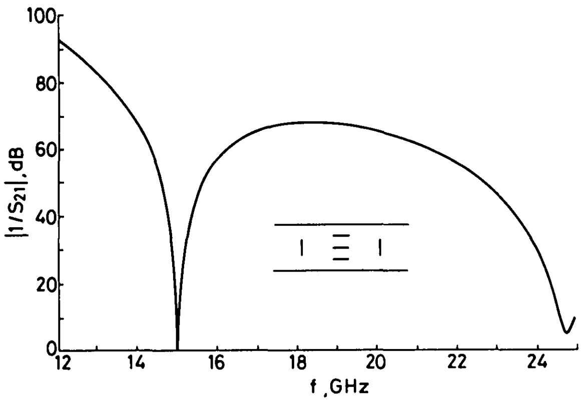

Fig. 9 *Filter composed of broadside oriented strip obstacles and a triple insert for coupling elements*

Filter dimensions:
Waveguide housing a = 15.799 mm, b = 7.899 mm (Ku-band, R140)
Obstacle, strip thickness t = 190 μm
Resonator lengths $l_{R1} = l_{R2}$ = 11.662 mm
Strip obstacle widths $w_1 = w_3$ = 5.28 mm
Triple-strip length l_1 = 4.966 mm, triple-strip spacing s = 3.759 mm

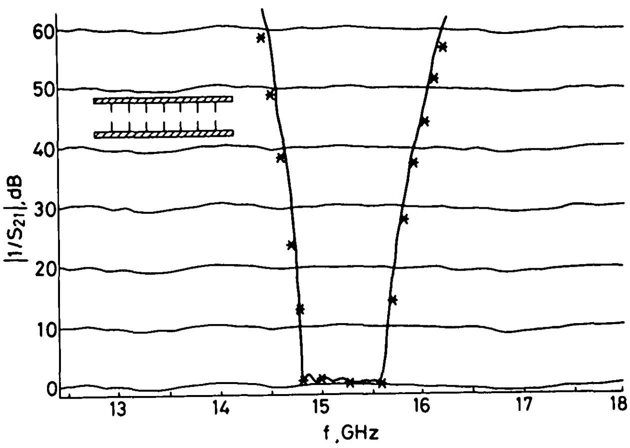

Fig. 10 *Calculated and measured insertion loss of an iris-coupled six-resonator filter*

Filter dimensions:
Waveguide housing a = 15.799 mm, b = 7.899 mm (Ku-band, R140)
Resonator lengths $l_{R1} = l_{R6}$ = 10.986 mm, $l_{R2} = l_{R5}$ = 11.868 mm, $l_{R3} = l_{R4}$ = 11.956 mm
Iris widths $w_1 = w_7$ = 6.204 mm, $w_2 = w_6$ = 3.888 mm, $w_3 = w_5$ = 3.604 mm, w_4 = 3.522 mm
Iris thickness t = 190 μm
——— measured
× × × theory

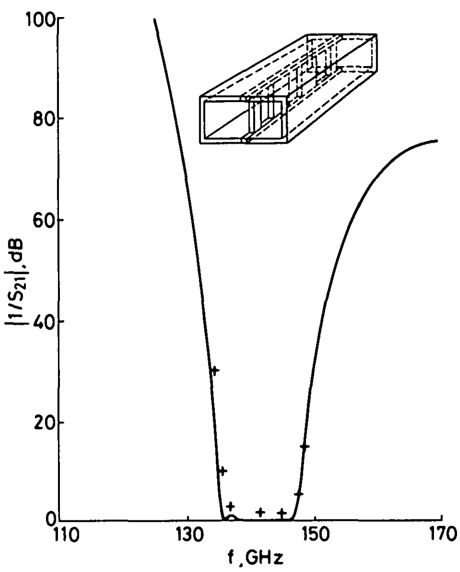

a

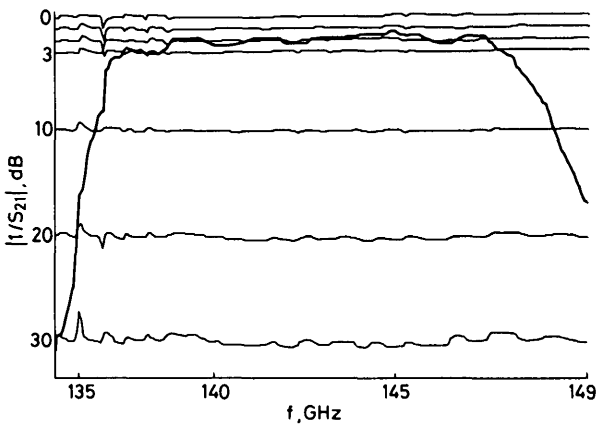

b

Fig. 11 *Broadband E-plane integrated metal-insert D-band filter with seven resonators*

a Calculated and measured insertion loss (mech. tolerances included)
Filter dimensions (cf. Fig. 1*b*):
Waveguide housing a = 1.651 mm, b = 0.826 mm
(D-band, R140);
Insert thickness t = 58 μm
Resonator lengths l_{R1} = 1.020 mm, $l_{R2} = l_{R3} = l_{R6}$ = 1.045 mm, l_{R4} = 1.035 mm, l_{R5} = 1.040 mm, l_{R7} = 1.010 mm
Insert lengths $l_1 = l_8$ = 0.070 mm, $l_2 = l_7$ = 0.350 mm, l_3 = 0.450 mm, $l_4 = l_5$ = 0.470 mm, l_6 = 0.440 mm
+ + + Measured $|1/s_{21}|_{min}$ = 1.4 dB
b Expanded view of measured insertion loss

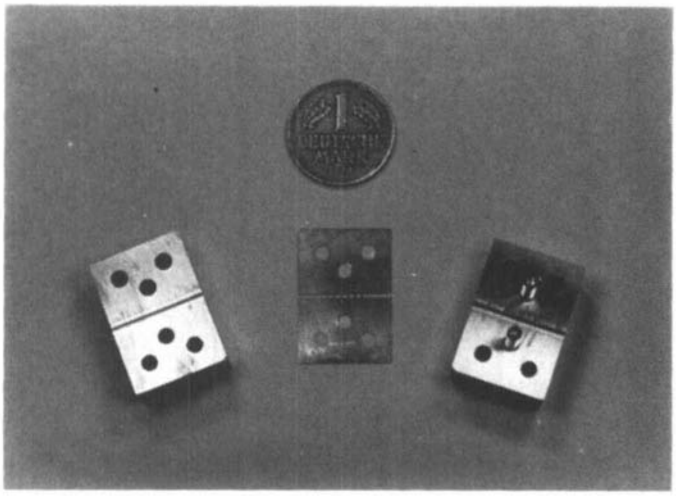

Fig. 12 *Seven-resonator D-band filter structure together with the opened waveguide housing*

loss of this filter, based on estimations of the unloaded Q of rectangular waveguide resonators given in Reference 3, is 0.27 dB, which compares well with the measured results presented in Fig. 10.

A broadband metal insert D-band (110–170 GHz) filter is shown in Fig. 11. The material of the 58 μm-thick inserts, again, is 99.9% pure copper. Fig. 12 shows the photograph of the seven-resonator filter structure, together with the opened waveguide housing. The insert is held in the split block by alignment pins.

The calculated midband dissipation loss of this filter is 1.3 dB, which compares well with measurements (Fig. 11*b*). This calculation was based on estimations of the unloaded Q using the measured finline resonator results of Reference 18 and the statements concerning dissipative losses of lowpass prototype filters given in Reference 3.

5 Conclusion

The modal S-matrix method described achieves the exact computer-aided design of inductively direct coupled cavity filters. Since the theory includes the finite thickness of the diaphragms, strips or posts, as well as the immediate higher-order mode interaction of all discontinuities, the stopband characteristic of the filter is taken into account in the optimisation process. Improved stopband attenuation is provided by cavities with modified width, and multiple E-plane inserts. The measured results verify the theory given by excellent agreement.

6 Acknowledgments

The D-band filter has been measured by AEG-Telefunken, Ulm, W.-Germany. The authors thank Dr. Menzel, the Head of the laboratory, and the members of his staff, especially Dipl.-Ing. Callsen, for this aid. Further, the authors acknowledge the financial support for parts of the research work by MBB/Erno, München, W. Germany, and thank Dr. Meck and Dr. Bätz for stimulating discussions.

7 References

1 MARCUVITZ, N.: 'Waveguide handbook' (McGraw-Hill, 1951), Chaps. 4 and 5

2 COHN, S.B.: 'Direct-coupled resonator filters'. *Proc. IRE*, 1957, **45**, pp. 187–196

3 MATHAEI, G.-L., YOUNG, L., and JONES, E.M.T.: 'Microwave filters, impedance-matching networks, and coupling structures' (McGraw-Hill, 1964), Chaps. 4, 5, 8, 9, 11

4 YOUNG, L.: 'Direct-coupled cavity filters for wide and narrow bandwidths', *IEEE Trans.*, 1963, **MTT-11**, pp. 162–178

5 LEVY, R.: 'Theory of direct-coupled-cavity filters', *ibid.*, 1967, **MTT-15**, pp. 340–348

6 LEVY, R.: 'Tables of element values for the distributed low-pass prototype filter', *ibid.*, 1965, **MTT-13**, pp. 514–536

7 LEVY, R., and RIBLET, H.J.: 'Improvement to theory of direct-coupled-cavity filters', *ibid.*, 1968, **MTT-16**, pp. 567–568

8 HAINE, J.L., and RHODES, J.D.: 'Direct design formulas for asymmetric bandpass channel diplexers', *ibid.*, 1977, **MTT-25**, pp. 807–813

9 RHODES, J.D., and ALSEYAB, S.A.: 'A design procedure for bandpass channel multiplexers connected at a common junction', *ibid.*, 1980, **MTT-28**, pp. 246–253

10 REED, J.: 'Precision design of direct coupled filters', *ibid.*, 1967, **MTT-15**, pp. 134–136

11 BRATHERTON, J.: 'Waveguide filters for mm wavelengths', *Microwave J.*, 1982, **25**, (7), pp. 91–95

12 GRAVEN, G., and LEWIN, L.: 'Design of microwave filters with quarter-wave couplings', *Proc. IEE*, 1956, **103B**, pp. 173–175

13 MARIANI, E.A.: 'Designing narrow-band triple-post waveguide filters', *Microwaves*, 1965, **4**, pp. 93–97

14 LI, P.G., ADAMS, A.T., LEVIATAN, Y., and PERINI, J.: 'Multiple-post inductive obstacles in rectangular waveguides', *IEEE Trans.*, 1984, **MTT-32**, pp. 365–373

15 AUDA, H., and HARRINGTON, R.F.: 'Inductive posts and diaphragms of arbitrary shape and number in a rectangular waveguide', *ibid.*, 1984, **MTT-32**, pp. 606–613

16 CHANG, K.: 'Impedance calculation of three resonant strips on the transverse plane of a rectangular waveguide', *ibid.*, 1984, **MTT-32**, pp. 126–130

17 MEIER, P.J.: 'Two new integrated-circuit media with special advantages at millimeter-wavelengths'. IEEE MTT-S International Microwave Symp. Digest, 1972, pp. 221–223

18 MEIER, P.J.: 'Integrated fin-line millimeter components', *IEEE Trans.*, 1974, **MTT-22**, pp. 1209–1216

19 KONISHI, Y., and UENAKADA, K.: 'The design of a bandpass filter with inductive strip — Planar circuit mounted in waveguide', *ibid.*, 1974, **MTT-22**, pp. 869–873

20 MEIER, P.J.: 'Planar multiport millimeter integrated circuits'. IEEE MTT-S International Microwave Symp. Digest, 1977, pp. 385–390

21 MEIER, P.J.: 'Millimeter integrated circuits suspended in the E-plane of rectangular waveguide', *IEEE Trans.*, 1978, **MTT-26**, pp. 726–733

22 MENZEL, W., CALLSEN, H., and SOLBACH, K.: 'An integrated receiver front-end for a 94 GHz dual polarisation radar'. Proc. 13th European Microwave Conf, Nürnberg, W. Germany, 1983, pp. 142–147

23 SOLBACH, K.: 'The status of printed millimeter-wave E-plane circuits', *IEEE Trans.*, 1983, **MTT-31**, pp. 107–121

24 MEIER, P.J.: 'Integrated fin-line: The second decade', *Microwave J.*, 1985, **28**, (11), pp. 31–54

25 VAHLDIECK, R., BORNEMANN, J., ARNDT, F., and GRAUERHOLZ, D.: 'Optimized waveguide E-plane metal insert filters for millimeter-wave applications', *IEEE Trans.*, 1983, **MTT-31**, pp. 65–69

26 BORNEMANN, J., ARNDT, F., VAHLDIECK, R., and GRAUERHOLZ, D.: 'Double planar integrated millimeter-wave filter'. Proc. 13th European Microwave Conf., Nürnberg, W. Germany, 1983, pp. 168–173

27 VAHLDIECK, R., BORNEMANN, J., ARNDT, F., and GRAUERHOLZ, D.: 'W-band low-insertion-loss E-plane filter', *IEEE Trans.*, 1984, **MTT-32**, pp. 133–135

28 BORNEMANN, J., VAHLDIECK, R., ARNDT, F., and GRAUERHOLZ, D.: 'Optimized low-insertion-loss millimetre-wave fin-line and metal insert filters', *Radio & Electron. Eng.*, 1982, **52**, pp. 513–521

29 ARNDT, F., BEIKE, J., GRAUERHOLZ, D., LINGEMANN, C., and BORNEMANN, J.: 'E-plane integrated parallel-strip screen waveguide filters', *IEEE Trans.*, 1985, **MTT-33**, pp. 654–659

30 ARNDT, F., BORNEMANN, J., PIONTEK, C., and SCHÜLER, H.: 'Shunt-inductance-coupled waveguide filters with expanded second stop-band', *Electron. Lett.*, 1985, **21**, pp. 238–239

31 PATZELT, H., and ARNDT, F.: 'Double plane steps in rectangular waveguides and their application for transformers, irises, and filters', *IEEE Trans.*, 1982, **MTT-30**, pp. 771–776

32 COLLIN, R.E.: 'Field theory of guided waves' (McGraw-Hill, 1960), Chap. 8

33 HARRINGTON, R.F.: 'Time harmonic electromagnetic fields' (McGraw-Hill, 1961), Chap. 8

34 WEXLER, A.: 'Solution of waveguide discontinuities by modal analysis', *IEEE Trans.*, 1967, **MTT-15**, pp. 508–517

35 MASTERMAN, P.H., CLARRICOATS, P.J.B., and HANNAFORD,

C.D.: 'Computer method of solving waveguide-iris problems', *Electron. Lett.*, 1969, **5**, (2), pp. 23–25
36 MASTERMAN, P.H., and CLARRICOATS, P.J.B.: 'Computer field-matching solution of waveguide transverse discontinuities', *Proc. IEE*, 1971, **118**, (1), pp. 51–63
37 LEE, S.W., JONES, W.R., and CAMPBELL, J.J.: 'Convergence of numerical solutions of iris-type discontinuity problems', *IEEE Trans.*, 1971, **MTT-19**, pp. 528–536
38 SAFAVI-NAINI, R., and MACPHIE, R.H.: 'On solving waveguide junction scattering problems by the conversation of complex power technique', *ibid.*, 1981, **MTT-29**, pp. 337–343
39 KNETSCH, H.D.: 'Beitrag zur Theorie sprunghafter Querschnittsveränderungen von Hohlleitern', *Arch. Elektron. & Übertragungstech.*, 1968, **AEÜ-22**, pp. 591–600
40 KNETSCH, H.D.: 'Anwendung der Methode der Orthogonalentwicklung bei unendlich dünnen Blenden in Hohlleitern', *ibid.*, 1969, **AEÜ-23**, pp. 361–368
41 DE SMEDT, R., and DENTURCK, B.: 'Scattering matrix of junctions between rectangular waveguides', *IEE Proc. H, Microwaves, Opt. & Antennas*, 1983, **130**, (2), pp. 183–190
42 ROZZI, T.E.: 'Equivalent network for interacting thick inductive irises', *IEEE Trans.*, 1972, **MTT-20**, pp. 323–330
43 ROZZI, T.E.: 'The variational treatment of thick interacting inductive irises', *ibid.*, 1973, **MTT-21**, pp. 82–88
44 YAMAMOTO, K.: 'Analysis and design of a millimeter-wave bandpass filter with a stopband in the specified higher frequencies', *ibid.*, 1976, **MTT-24**, pp. 837–842
45 ARNDT, F., and PAUL, U.: 'The reflection definition of the characteristic impedance of microstrips', *ibid.*, 1979, **MTT-27**, pp. 724–730
46 SCHMIEDEL, H.: 'Anwendung der Evolutionsoptimierung auf Schaltungen der Nachrichtentechnik', *Frequenz*, 1981, **35**, pp. 306–310
47 NAVARRO, M.S., ROZZI, T.E., and LO, Y.T.: 'Propagation in a rectangular waveguide periodically loaded with resonant irises', *IEEE Trans.*, 1980, **MTT-28**, pp. 857–867
48 ROZZI, T.E., and MECKLENBRÄUKER, W.F.G.: 'Wide-band network modeling of interacting inductive irises and steps', *ibid.*, 1975, **MTT-23**, pp. 235–245
49 SHIH, Y.-C., ITOH, T., and BUI, L.Q.: 'Computer-aided design of millimeter-wave E-plane filters', *ibid.*, 1983, **MTT-31**, pp. 135–142
50 BUI, L.Q., BALL, D., and ITOH, T.: 'Broad-band millimeter-wave E-plane Bandpass filters', *ibid.*, 1984, **MTT-32**, pp. 1655–1658

8 Appendix

8.1 Abbreviations in eqn. 2

Discontinuity change in width (Fig. 2*a*) $v = \mathrm{I}, \mathrm{II}$:

$$f^{(v)} = (x - x_1, x - x_0)^T \quad (T = \text{transposed}) \tag{12}$$

$$p^{(v)} = (x_2 - x_1, x_3 - x_0)^T \tag{13}$$

Discontinuity waveguide N-furcation (Fig. 2*c*) $v = \mathrm{I}, \mathrm{II1}, \mathrm{II2}, \mathrm{II3}, \ldots, \mathrm{IIi}, \ldots, \mathrm{IIN}$:

$$f^{(v)} = (x, x, x - m_1, \ldots, x - m_{i-1}, \ldots, x - m_{N-1})^T \tag{14}$$

$$p^{(v)} = (a, p_1, p_2 - m_1, \ldots, p_i - m_{i-1}, \ldots, a - m_{N-1})^T \tag{15}$$

For the two discontinuities, T_m is given by

$$T_m^{(v)} = \frac{1}{k_{zm}^{(v)}\sqrt{[\omega\mu k_{zm}^{(v)}]}} \cdot \sqrt{\left[\frac{2}{b \cdot p^{(v)}}\right]} \tag{16}$$

where b is the waveguide height and

$$k_{zm}^{(v)2} = \omega^2 \mu \varepsilon^{(v)} - \left(\frac{m\pi}{p^{(v)}}\right)^2 \tag{17}$$

is the propagation factor of the mth mode in the waveguide subregion v.

8.2 Submatrices in eqn. 3

$$(S_{11}^W) = (\boldsymbol{W})^{-1}[(\boldsymbol{U}) - (\boldsymbol{L}_H)(\boldsymbol{L}_E)]$$
$$(S_{12}^W) = 2(\boldsymbol{W})^{-1}(\boldsymbol{L}_H)$$
$$(S_{21}^W) = (\boldsymbol{L}_E)\{(\boldsymbol{W})^{-1}[(\boldsymbol{U}) - (\boldsymbol{L}_H)(\boldsymbol{L}_E)] + (\boldsymbol{U})\}$$
$$(S_{22}^W) = 2(\boldsymbol{L}_E)(\boldsymbol{W})^{-1}(\boldsymbol{L}_H) - (\boldsymbol{U}) \tag{18}$$

where

$$(\boldsymbol{W}) = (\boldsymbol{U}) + (\boldsymbol{L}_H)(\boldsymbol{L}_E)$$

and

$$(\boldsymbol{U}) = \text{unit matrix}$$

the matrix coefficients of $\boldsymbol{L}_E$ are given by

$$L_{Emn} = 2\sqrt{\left[\frac{k_{zm}^{(\mathrm{II})}}{(x_3 - x_0)(x_2 - x_1)k_{zm}^{(\mathrm{I})}}\right]} \cdot \int_{x_1}^{x_2} \sin\left\{\frac{m\pi}{x_3 - x_0}(x - x_0)\right\} \cdot \sin\left\{\frac{n\pi}{x_2 - x_1}(x - x_1)\right\} dx$$

$(\boldsymbol{L}_H)$ is the transposed matrix

$$(\boldsymbol{L}_H) = (\boldsymbol{L}_E)^T$$

8.3 Scattering coefficients of two series connected structurers with the scattering matrices $(\boldsymbol{S})^{(1)}$ and $(\boldsymbol{S})^{(2)}$

$$(S_{11})^{total} = (S_{11})^{(1)} + (S_{12})^{(1)} \cdot [(\boldsymbol{U}) - (S_{11})^{(2)}(S_{22})^{(1)}]^{-1}(S_{11})^{(2)}(S_{21})^{(1)}$$
$$(S_{12})^{(total)} = (S_{12})^{(1)}[(\boldsymbol{U}) - (S_{11})^{(2)}(S_{22})^{(1)}]^{-1} \cdot (S_{12})^{(2)}$$
$$(S_{21})^{(total)} = (S_{21})^{(2)}[(\boldsymbol{U}) - (S_{22})^{(1)}(S_{11})^{(2)}]^{-1} \cdot (S_{21})^{(1)}$$
$$(S_{22})^{(total)} = (S_{21})^{(2)}[(\boldsymbol{U}) - (S_{22})^{(1)}(S_{11})^{(2)}]^{-1} \cdot (S_{22})^{(1)}(S_{12})^{(2)} + (S_{22})^{(2)} \tag{19}$$

U is the unity matrix.

8.4 Submatrices in eqn. 7

$$(S_{11}^I) = (S_{22}^I) = (S_{11}^B) + (S_{12}^B)[(\boldsymbol{U}) - (\boldsymbol{E})(S_{11}^W)(\boldsymbol{E})(S_{22}^B)]^{-1} \cdot (\boldsymbol{E})(S_{11}^W)(\boldsymbol{E})(S_{21}^B)$$
$$(S_{12}^I) = (S_{21}^I) = (S_{12}^B)[(\boldsymbol{U}) - (\boldsymbol{E})(S_{11}^W)(\boldsymbol{E})(S_{22}^B)]^{-1} \cdot (\boldsymbol{E})(S_{12}^W) \tag{20}$$

8.5 Submatrices in eqn. 9

$$(S_{11}^0) = (S_{22}^0) = -[(\boldsymbol{U}) + (\boldsymbol{P}) - (\boldsymbol{Q}) \cdot ((\boldsymbol{U}) + (\boldsymbol{P}))^{-1} \cdot (\boldsymbol{Q})]^{-1} \cdot [(\boldsymbol{U}) - (\boldsymbol{P}) + (\boldsymbol{Q}) \cdot ((\boldsymbol{U}) + (\boldsymbol{P}))^{-1} \cdot (\boldsymbol{Q})]$$
$$(S_{12}^0) = (S_{21}^0) = -[(\boldsymbol{U}) + (\boldsymbol{P}) - (\boldsymbol{Q}) \cdot ((\boldsymbol{U}) + (\boldsymbol{P}))^{-1} \cdot (\boldsymbol{Q})]^{-1} \cdot [(\boldsymbol{Q}) + (\boldsymbol{Q}) \cdot ((\boldsymbol{U}) + (\boldsymbol{P}))^{-1} \cdot ((\boldsymbol{U}) - (\boldsymbol{P}))] \tag{21}$$

with

$$(P) = \sum_{\eta=1}^{N} (\boldsymbol{L}^{(\eta)})[(\boldsymbol{U}) - 2((\boldsymbol{R}^{(\eta)}) - (\boldsymbol{R}^{(\eta)})^{-1})^{-1} \cdot (\boldsymbol{R}^{(\eta)})] \cdot (\boldsymbol{M}^{(\eta)}) \tag{22}$$

$$(Q) = \sum_{\eta=1}^{N} (\boldsymbol{L}^{(\eta)})[2((\boldsymbol{R}^{(\eta)}) - (\boldsymbol{R}^{(\eta)})^{-1})^{-1}](\boldsymbol{M}^{(\eta)}) \tag{23}$$

$(\boldsymbol{U})$ = unity matrix

where $(\boldsymbol{R}^{(\eta)}$ is the diagonal matrix of the N-furcated waveguide section of length l (Fig. 2c) with m modes considered

$$\begin{pmatrix} e^{-jk_{z1}^{\mathrm{II}(\eta)} \cdot l} & & 0 \\ & e^{-jk_{z2}^{\mathrm{II}(\eta)} \cdot l} & \\ & & \ddots \; e^{-jk_{zm}^{\mathrm{II}(\eta)} \cdot l} \\ 0 & & \end{pmatrix} \tag{24}$$

$(\boldsymbol{L}^{(\eta)})$ is the matrix containing the coupling integrals with the elements

$$L_{ij}^{(\eta)} = H_{ij}^{(\eta)} \frac{2}{\sqrt{[a(p_\eta - m_{\eta-1})]}} \sqrt{\left[\frac{k_{zi}^{(\mathrm{I})}}{k_{zj}^{(\mathrm{II}\eta)}}\right]} \tag{25}$$

$$H_{ij}^{(\eta)} = \int_{m_{\eta-1}}^{p_\eta} \left(\sin \frac{i\pi}{a} x\right) \cdot \left(\sin \frac{j\pi}{p_\eta - m_{\eta-1}} (x - m_{\eta-1})\right) dx \tag{26}$$

and the matrix

$$(\boldsymbol{M}^{(\eta)}) = (\boldsymbol{L}^{(\eta)})^T$$